

INFRARED SPECTROSCOPY OF SYMBIOTIC STARS. VI. COMBINED ORBITS FOR TWO S-TYPE SYSTEMS: V455 SCORPII AND SS 73-90

FRANCIS C. FEKEL^{1,5}, KENNETH H. HINKLE², RICHARD R. JOYCE², PETER R. WOOD³, AND IAN D. HOWARTH⁴

¹ Center of Excellence in Information Systems, Tennessee State University, Nashville, TN, USA; fekel@evans.tnstate.edu

² National Optical Astronomy Observatory, Tucson, AZ, USA; hinkle@noao.edu, joyce@noao.edu

³ Research School of Astronomy and Astrophysics, Mount Stromlo Observatory, Australian National University, Canberra, ACT, Australia; wood@mso.anu.edu.au

⁴ Department of Physics and Astronomy, University College London, London, UK; idh@star.ucl.ac.uk

Received 2007 December 17; accepted 2008 April 18; published 2008 June 3

ABSTRACT

We have combined new infrared radial velocities and previously obtained spectropolarimetric observations to compute orbits of the M6 giants in two southern S-type symbiotic systems. The spectropolarimetric data enable the orbital inclinations of the systems to be determined, placing greater constraints on the properties of the components. V455 Sco has a circular orbit with a period of 1398 ± 6 days and an inclination of $94^\circ \pm 1^\circ$. The orbit of SS 73-90 has a period of 898 ± 5 days, a modest eccentricity of 0.16, and an inclination of $97^\circ \pm 7^\circ$. The center of mass velocity of each system is large, -77.9 km s^{-1} for V455 Sco and 89.5 km s^{-1} for SS 73-90, making them members of the old disk population. The M giant component of each system is likely on the asymptotic giant branch. From estimates of the M giants' radii we predict that both systems are eclipsing and provide ephemerides to search for the eclipses. For V455 Sco, the predicted eclipses are found in data from the Harvard College Observatory plate archives. The He II emission feature near $1.0123 \mu\text{m}$ is associated with the hot component in both systems. However, the orbits produced from the emission-line radial velocities do not lead to masses that are consistent with other results.

Key words: binaries: symbiotic – infrared: stars – stars: individual (V455 Sco, SS 73-90) – stars: late-type

1. INTRODUCTION

About 75 years ago Berman (1932) and Hogg (1934) suggested that the peculiar combination spectra of the stars now given the appellation *symbiotics* could be explained by a binary star. However, it took over a half century before the true nature of these systems became clear. Visual and ultraviolet spectroscopy finally showed conclusively that symbiotic stars are mass-transfer binaries, consisting of a cool giant and a hot star (Kenyon & Webbink 1984; Garcia 1986; Mürset et al. 1991). Usually the companion of the K or M giant appears to be a compact object, either a white dwarf or at least in one case (Hinkle et al. 2006) a neutron star, but in a few systems it may be a low-mass, main-sequence star. From their characteristics at infrared wavelengths Webster & Allen (1975) separated the symbiotics into two subclasses, D for dusty-type and S for stellar-type systems. The S-type symbiotics have typical orbital periods of 2–3 yr, while those of the D-type systems are at least an order of magnitude longer (Schmid & Schild 2002). Fekel et al. (2000b) and Mikołajewska (2003) have provided a more extensive introduction to this group of stars.

Orbital elements of the late-type giant component provide a major starting point for an understanding of symbiotic systems. However, veiling and numerous emission lines contaminate the spectra of the giants at blue wavelengths. To alleviate such problems, observations to detect the K or M giant component are best made at infrared wavelengths. In addition, the stars are faint, with $\sim 50\%$ of the confirmed symbiotics in the catalog of Belczyński et al. (2000) having $V \geq 13.0$ mag, so in general, moderate aperture telescopes are required to obtain high-resolution spectra from which precise radial velocities can be determined. High precision is needed because the long orbital

periods of the systems result in low velocity amplitudes. Such properties make well-determined orbital elements difficult to obtain. As a result, of the nearly 200 symbiotic systems listed in the recent catalog of Belczyński et al. (2000), only 30 systems or about 15% have had spectroscopic orbital elements determined for the cool giant component (Mikołajewska 2003; Fekel et al. 2007). In five previous papers in this series (Fekel et al. 2000a, 2000b, 2001, 2007; Hinkle et al. 2006) we have determined the orbital elements for the late-type component in 18 systems, seven of which are first orbits.

The present work provides the first spectroscopic orbits for the late-type giant components in two more S-type symbiotics, V455 Sco and SS 73-90. Because of the general faintness of the objects in this class, there are name identification issues. The latter system does not have a variable star name, and so we have chosen to use the designation SS 73-90 from the list of Sanduleak & Stephenson (1973), who identified the star as a symbiotic system, rather than earlier designations of M1-21 and Hen 2-247 from two other surveys, where the system was identified as a planetary nebula. To make things even more complicated, none of these three names is the primary identification given by SIMBAD, which instead uses an even more esoteric name, ESO 588-7. The catalog of Belczyński et al. (2000) is helpful in this regard because it provides a variety of alternative designations.

Harries & Howarth (2000) previously determined provisional orbital parameters for V455 Sco and SS 73-90 from spectropolarimetric observations. Combining those observations with our radial velocities, we have obtained orbits with a more extensive set of elements for the two binaries. This is because the spectropolarimetric observations map polarization position angle and magnitude on the plane of the sky and hence provide two additional orbital elements that cannot be determined from the radial velocities: the inclination, i , and the position angle of the line of nodes, Ω .

⁵ Visiting Astronomer, Kitt Peak National Observatory, National Optical Astronomy Observatory, operated by the Association of Universities for Research in Astronomy, Inc., under cooperative agreement with the National Science Foundation.

Table 1
Basic Properties of the Program Stars

Name	V^a (mag)	K^a (mag)	$H - K^a$ (mag)	Primary spectral class ^b	Orbital period (days)	\dot{M}^c ($M_{\odot} \text{ yr}^{-1}$)
V455 Sco	13.73	5.99	0.43	M6.5	1398	1.7×10^{-6}
SS 73-90	13.52	7.03	0.40	M6	898	1.7×10^{-7}

Notes.

^a Munari et al. (1992).

^b Mürset & Schmid (1999).

^c Seaquist et al. (1993).

Because the systems reside in the southern sky, these symbiotic stars have not been as extensively observed as most of their northern brethren. It is hoped that the determination of the improved orbits and the resulting ephemerides for eclipses will lead to more intensive observing of these symbiotics. Some basic information for the two systems is listed in Table 1.

2. OBSERVATIONS AND REDUCTIONS

2.1. Spectroscopic

From 2001 March to 2007 June we obtained 18 spectroscopic observations of V455 Sco. The first eight were obtained with the 1.88 m telescope and coudé spectrograph system at the Mount Stromlo Observatory (MSO), Canberra, Australia. The detector was an infrared camera, NICMASS, developed at the University of Massachusetts. We obtained a 2 pixel resolving power of 44,000 at a wavelength of 1.623 μm . A more complete description of the experimental setup may be found in Joyce et al. (1998), as well as in Fekel et al. (2000b). The detector and electronics were previously used for our survey of northern symbiotics, carried out with the coudé feed telescope at Kitt Peak National Observatory (KPNO).

The devastating bush fire of 2003 January destroyed both the 1.88 m telescope at MSO and our infrared NICMASS camera. On four dates between 2003 February and 2004 April we were able to continue observations using the Phoenix cryogenic echelle spectrograph, mounted on the 8 m Gemini South telescope at Cerro Pachon, Chile. A complete description of the spectrograph can be found in Hinkle et al. (1998). The first two Gemini South observations were centered at 1.563 or 2.226 μm , a region containing several atomic lines, and have a resolving power of 50,000. The final spectrogram was also centered at 2.226 μm but has a somewhat higher resolving power of $\sim 70,000$. The wavelength and resolution were selected to allow detailed analysis of line profiles. These data were taken for a separate program on symbiotic abundances as well as the current radial-velocity work.

The seven most recent observations were acquired from 2004 May to 2007 June at KPNO with the 0.9 m coudé feed telescope, coudé spectrograph, and a CCD, designated LB1A. This 1980 \times 800 pixel CCD was manufactured by Lawrence Berkeley National Laboratory and is 300 μm thick. Although this thickness results in increased pixel contamination by cosmic ray and background radiation events, the chip was used because of its high quantum efficiency at far-red wavelengths. Our spectrograms, centered near 1.005 μm , have a wavelength range of 420 Å, and a resolving power of $\sim 21,500$.

The observing history of SS 73-90 is similar to that of V455 Sco. Over a 6 yr period we collected 17 spectroscopic observations of SS 73-90. From 2001 May through 2002 August, we acquired six spectrograms at MSO with the same telescope,

spectrograph, and infrared camera that were used for V455 Sco. After the loss of our instrument and the MSO facility, from 2003 February through 2004 April we obtained four observations with the 8 m Gemini South telescope and the Phoenix spectrograph. We completed our observations at KPNO with seven more spectrograms, acquired from 2004 May to 2007 June. For those observations we used the coudé feed telescope, coudé spectrograph, and LB1A CCD detector.

Standard observing and reduction techniques were used (Joyce 1992). Wavelength calibration at the infrared wavelengths of 1.563 and 2.223 μm posed a challenge, because the spectral coverage was far too small to include a sufficient number of ThAr emission lines for a dispersion solution. Thus, at 1.563 μm our approach was to utilize the absorption lines of a bright late-type giant star. Depending on the observing run, HR 3718, β Oph, δ Oph, or α Cet was observed. Approximately 20 lines of CN, Fe, and OH were used to calculate the dispersion solution in this wavelength region. Each solution was offset to an absolute standard provided by one or more telluric OH emission lines. At 2.223 μm the wavelength calibration was done by measuring telluric absorption lines in the spectrum of β Lup, a bright early-type star. The typical root mean square (rms) of the solutions for both regions was about 0.02 Å.

For the spectrograms acquired with the LB1A CCD at 1.005 μm , we were able to use ThAr spectra for the wavelength calibration. Telluric lines are present in the 1.005 and 2.223 μm wavelength regions. These lines were removed from our observations by ratioing the spectra to a hot star spectrum observed on the same night.

Representative spectra of the two program stars at wavelengths of 1.005, 1.563, and 2.223 μm are shown in Figures 1–3, respectively. Spectra of our velocity standard δ Oph, which has a spectral type of M0.5 III (Keenan & McNeil 1989), have been included for comparison in each of the three figures. All three regions are dominated by absorption lines arising in the photosphere of the red giant. The 1.005 μm region has a number of neutral atomic lines present, especially from Ti and Fe. There are also many weak-to-moderate strength lines from bands of the $\Delta v = -1$ CN red system. Unlike the two spectral regions farther to the red, the one centered on 1.005 μm also contains some emission features associated with the symbiotic mass transfer. The 1.563 μm region is dominated by OH first overtone lines and a selection of neutral atomic lines and also has weak CN red-system $\Delta v = -1$ lines and CO vibration-rotation second-overtone lines. The 2.223 μm region contains moderately strong Ti I lines as well as a few other neutral atomic lines, especially from Fe I and Sc I. The CN red-system $\Delta v = -2$ transition provides a background of weak lines.

Absorption-line radial velocities of the two program stars were measured with the IRAF cross-correlation program FXCOR (Fitzpatrick 1993). The velocities were determined

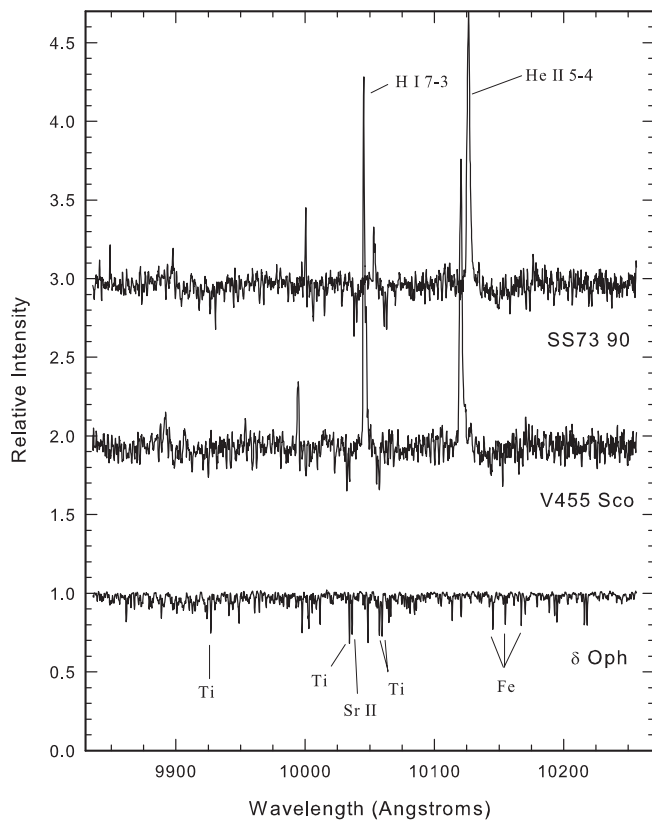


Figure 1. Spectra of the two program stars and velocity standard δ Oph at $1.005 \mu\text{m}$ observed with the KPNO coude feed telescope, spectrograph, and LB1A CCD. The entire observed spectral region is shown. The telluric spectrum has been ratioed out by referencing a hot star spectrum acquired on the same night. The relative intensity scales for V455 Sco and SS 73-90 have been offset by 1.0 and 2.0, respectively. A few of the stronger representative absorption and emission lines are identified. For V455 Sco, the relative intensities of two emission features are so strong that they extend through the plotted spectrum of SS 73-90.

relative to the M giant International Astronomical Union velocity standard δ Oph, which was observed multiple times during the course of each night. Its radial velocity of -19.1 km s^{-1} was adopted from the work of Scarfe et al. (1990).

As noted above, several emission features are obvious in our spectra of the $1.005 \mu\text{m}$ region (Figure 1). However, only two could be readily identified: the Paschen δ line at $1.004938 \mu\text{m}$ and the He II line at $1.012361 \mu\text{m}$. Radial velocities of those two lines were measured with the IRAF task RVIDLINES. A Gaussian function was fitted to each emission line and the wavelength shift of the spectral feature relative to its rest wavelength was converted into a radial velocity, which was then corrected for the earth's motion. While many of the emission lines are relatively symmetric, in other cases the emission features are asymmetric or have two partially resolved components. When appropriate, two or three Gaussians were used to fit the blended features.

2.2. Spectropolarimetric

We have also used the spectropolarimetric observations of V455 Sco and SS 73-90 that were obtained by Harries & Howarth (2000). In that paper they described where and how the observations were collected and gave a brief summary of their data reduction procedures. Harries & Howarth (1996) provided additional details about their observing techniques and data reduction.

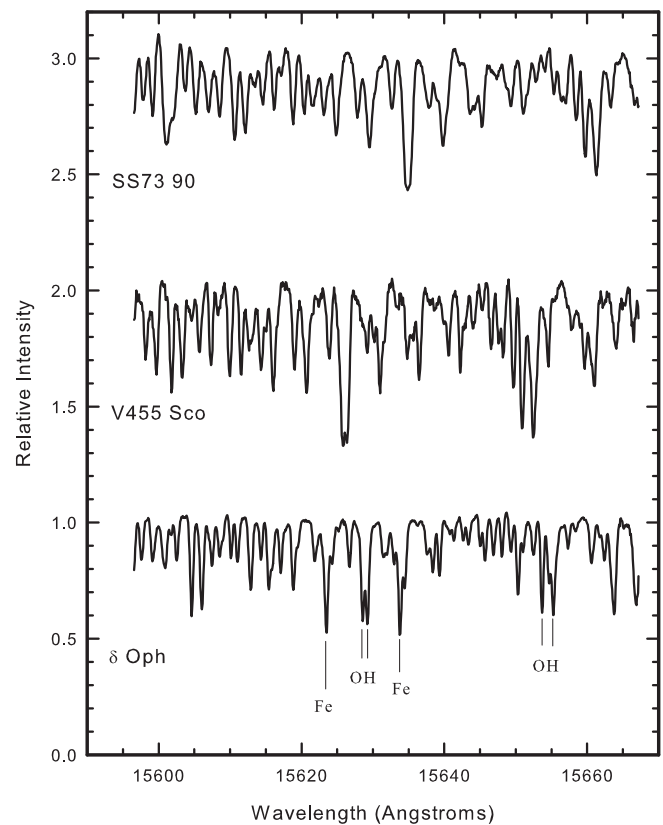


Figure 2. Spectra of the two program stars and δ Oph at $1.563 \mu\text{m}$ observed with Gemini South and the Phoenix spectrograph. This spectral region is not contaminated by telluric lines. The relative intensity scales for the symbiotic stars have been offset as in Figure 1.

3. ORBITAL ANALYSIS METHODOLOGY

Spectroscopic orbital elements of the two systems were determined with various computer programs. First, a preliminary period was identified with a program named PeriodoGRAM (PGRAM). An extensive range of periods was searched by computing the phases of the observed velocities for each trial period and comparing those phased velocities to a sine curve fit. The sum of the squared velocity residuals from the sine curve fit was computed, and the period having the smallest value of that sum was adopted as the best preliminary period. With this period identified, initial orbital elements were determined with BISP, a computer program that implements a slightly modified version of the Wilsing–Russell method (Wolfe et al. 1967). A differential corrections program, called SB1, of Barker et al. (1967) was used to refine the eccentric orbits of the single-lined systems. For each system, the orbital eccentricity is small enough that a circular-orbit solution may be appropriate. Such orbits were computed with SB1C (D. Barlow 1998, private communication), which also uses differential corrections to determine the orbital elements.

To obtain a joint orbital solution of the radial-velocity and spectropolarimetry measurements, we utilized a program called SYMGENI, which searches for solutions with the use of a genetic algorithm that employs the general-purpose optimization subroutine PIKAIA (Charbonneau 1995). A period search is an integral part of the general exploration of parameter space. Parameter errors were generated with SYMGENI by a Monte Carlo technique, adding offsets to the original measurements that were drawn from Gaussian probability distributions with dispersions based on residuals from the fits.

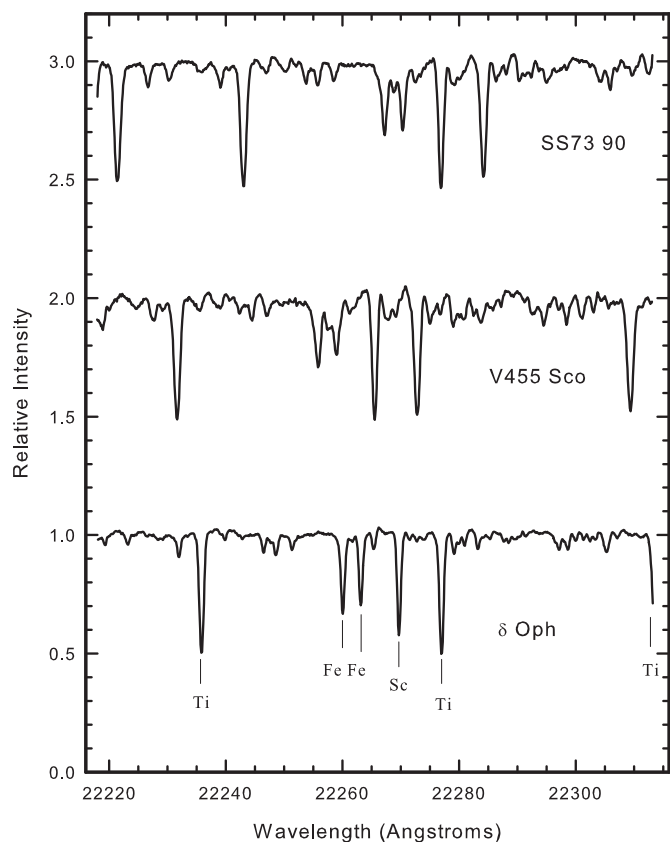


Figure 3. Spectra of the two program stars and δ Oph at $2.223 \mu\text{m}$ observed with Gemini South and the Phoenix spectrograph. The telluric spectrum has been ratioed out by referencing a hot star spectrum acquired on the same night. The relative intensity scales for the symbiotic stars have been offset as in Figure 1.

The relative weighting of the radial-velocity and spectropolarimetric observations affects the detailed numerical results of the fits. This presents a potential difficulty, since the weights depend on errors that are most straightforwardly estimated from residuals to the adopted solutions, while those solutions themselves depend on the weights. However, we emphasize that the general characteristics of the solutions are quite robust to the weighting schemes.

As discussed in Section 4, the residuals of the absorption-line radial-velocity solutions indicate that up to one-half of the velocity rms likely results from pulsational velocity variations, but we are unable to account specifically for them. We therefore retain the uncertainties of roughly 1 km s^{-1} for the velocity measurements. Solutions of the spectropolarimetry alone typically yield residuals that are several times larger than the formal statistical errors (see, e.g., Harries & Howarth 2000). Since, in common with other authors, we also find that emission-line radial velocities are unreliable tracers of orbital motion (see Sections 5.4 and 6.4), it seems prudent to regard the spectropolarimetric data, derived from emission-line measurements, as an innately less secure tracer of orbital motion than the absorption-line velocities. Our general weighting strategy was therefore to fix the errors of the absorption-line radial-velocity measurements at the level inferred from the velocity-only orbits, and vary the adopted uncertainties of the polarimetric measures until they agreed with the dispersion of the observations around the resulting joint solution.

4. PULSATION PERIOD SEARCH

As summarized by Percy et al. (2001), all M giants have light variability from pulsation at some level and the amplitude of such variability generally increases with later spectral type and higher luminosity. Most variables on the asymptotic giant branch (AGB) have relatively small amplitudes, and Lebzelter & Hinkle (2002) noted that the periods of these semi-regular variables typically range from 30 to 200 days. Velocity variations in semi-regular variables accompany the light variability and usually having amplitudes of up to a few km s^{-1} (e.g., Lebzelter & Hinkle 2002). Thus, given the M6 spectral classes of the giants in our two symbiotic binaries and our conclusion that the giants are on the AGB (Sections 5.5 and 6.5), a portion of the radial-velocity variations results from pulsation. However, as we note in Sections 5.5 and 6.5, there are almost no photometric observations for V455 Sco and SS 73-90, so we have no information about the periods of their pulsational variability. Comparing the results for the two systems in this paper with our symbiotic orbits with the smallest velocity residuals (Fekel et al. 2000b, 2001), we estimate that up to half of the rms error found for the radial-velocity orbital solutions of V455 Sco and SS 73-90 is due to pulsation. Thus, we examined the velocity residuals for periodicities.

Using PGRAM, we searched the residuals for periods between 10 and 500 days. The best period for V455 Sco was 22.5 days, while for SS 73-90 the two best periods were around 25 days. The luminosities of the two stars, determined in Sections 5.5 and 6.5, enable us to place the stars on the period–luminosity diagram for local M giants constructed by Glass & van Leeuwen (2007). For stars with the luminosities of our two symbiotics there is no evidence of significant light variability with periods as short as 20–30 days; longer periods are required. Indeed, our best possible periods may well be spurious because the frequency of our velocity observations, two or three per year for several years, produces a total of less than 20 velocities that are poorly spaced to determine such short periods. In addition, the amplitudes of our best periods are very low, only $2\text{--}3 \text{ km s}^{-1}$, so the best periods are heavily dependent on the placement of the few velocities with the largest residuals. Thus, we conclude that although both giants likely have modest velocity variability due to pulsation, it is impossible to determine the true periods from our limited number of velocities and thus remove the pulsational variations from our data.

$$5. \text{V455SCO} = \text{AS217} = \text{WRAY16} - 252 = \text{SS73} - 74 = \text{HEN3} - 1334$$

5.1. Short History

In a search for variable stars near the Galactic equator, Swope (1940) analyzed the Harvard College Observatory photographic plates. As a result, she discovered the irregular variable that was designated HV 7869 and later given the variable star name V455 Sco.

Merrill & Burwell (1950) listed this star as one of 519 “additional stars” with $\text{H}\alpha$ in emission that was found on Mount Wilson objective-prism plates, and so it became known as AS 217. They characterized it as having very strong $\text{H}\alpha$ emission, and in the notes to their Table 1, they reported that it had a peculiar and probable combination spectrum. This led Bidelman (1954) to place it in a list of stars with combination spectra, which included many symbiotic stars. Henize (1967) obtained objective-prism spectra of the sky south of declination -25° to identify $\text{H}\alpha$ emission line objects. From the long-exposure

plates of that survey Wray (1966) confirmed the $H\alpha$ emission, and it received the designation Wray 16-252. Wackerling (1970) included V455 Sco in a catalog of early-type stars with emission lines and listed it as a symbiotic star. Using objective-prism spectra, Sanduleak & Stephenson (1973) surveyed the southern Milky Way to search for luminous and emission-lined stars. They identified star number 74 in their 1973 list as a Z-Andromodae-like star, which had He II emission at 4686 Å that was significantly stronger than $H\beta$ emission. Three years later, Henize (1976) published a catalog of over 1900 southern, $H\alpha$ emission line stars, identified from objective-prism spectra that had been obtained about 25 years earlier in South Africa. Designated as Hen 3-1334, it was listed with other symbiotic stars although it was noted that TiO bands were not visible. Following up on the work of Sanduleak & Stephenson (1973), Allen (1978) acquired a low-dispersion slit spectrum of V455 Sco. He confirmed that it was a symbiotic star, noting its moderate TiO absorption and a rich emission-line spectrum.

Allen (1980) first classified V455 Sco as M6 from a spectrum at 2 μm . Medina Tanco & Steiner (1995) determined a spectral class of M6 from a visual comparison of its red wavelength region with standard star spectra, while Mürset & Schmid (1999) estimated a slightly later class of M6.5, which we have adopted (Table 1), from an analysis of the strength of several near-infrared wavelength TiO bandheads. Mikołajewska et al. (1997) found a spectral class of M1, seemingly at odds with the other results, but they noted that their spectral class must be considered an upper limit, and a later subclass was likely. Mikołajewska et al. (1997) also provided a limited analysis of V455 Sco, estimating the hot component temperature and luminosity plus the system distance.

V455 Sco was included in the symbiotic star catalog of Allen (1984), where a low-dispersion spectrum was shown, as well as the more recent catalog of Belczyński et al. (2000). The latter listed the spectroscopic orbital elements of 20 symbiotics, but V455 Sco was not one of those stars. However, at about the same time, Harries & Howarth (2000) published preliminary orbital solutions for V455 Sco from analyses of their spectropolarimetric observations. Presenting both a circular and an eccentric orbit, they preferred the circular one, which has a period of 1419 days.

5.2. Spectroscopic Orbit

From 2001 March to 2007 June we obtained 18 absorption-line radial velocities of V455 Sco (Table 2), which cover about 1.6 orbital cycles. An analysis of these velocities resulted in an initial period of 1445 days, in good agreement with the value of 1419 days found by Harries & Howarth (2000) for their circular-orbit solution. Adopting the period of 1445 days, we obtained preliminary orbital elements with BISP, which were then refined with SB1. That solution produced an orbit with a period of 1439 days and an eccentricity of 0.044 ± 0.075 . Because of this low orbital eccentricity and its greater uncertainty, we used SB1C to determine a circular-orbit solution, which has a period of 1443 days. The tests of Lucy & Sweeney (1971) indicated that the circular-orbit solution is to be preferred, so it is listed in Table 3. However, given the relatively long orbital period of nearly 4 yr, we caution that it is possible that the system still has a small eccentricity. Because a time of periastron passage, T , is undefined for a circular orbit, as recommended by Batten et al. (1989), we have instead listed T_0 , a time of maximum velocity, in the orbital elements table. The standard error of an individual velocity is 1 km s^{-1} .

Table 2
Radial Velocities of V455 SCO

HJD 2,400,000 +	Phase	Velocity (km s^{-1})	$O - C$ (km s^{-1})	Observatory
51,994.224	0.287	-80.1	-0.4	MSO
52,045.275	0.323	-83.3	-1.9	MSO
52,094.157	0.358	-83.0	-0.1	MSO
52,131.069	0.385	-84.2	-0.4	MSO
52,354.202	0.544	-85.2	0.3	MSO
52,398.302	0.576	-83.6	1.3	MSO
52,447.026	0.611	-84.4	-0.4	MSO
52,502.909	0.651	-82.4	0.1	MSO
52,687.863	0.783	-74.1	2.2	Gemini S
52,749.788	0.827	-74.1	0.1	Gemini S
53,098.797	0.077	-70.6	0.3	Gemini S
53,129.883	0.099	-72.5	-1.0	KPNO
53,178.852	0.134	-70.5	2.1	KPNO
53,493.913	0.360	-83.0	-0.1	KPNO
53,537.815	0.391	-84.0	0.0	KPNO
53,859.925	0.622	-83.9	-0.3	KPNO
54,230.787	0.887	-73.4	-1.5	KPNO
54,270.822	0.916	-71.5	-0.4	KPNO

5.3. Combined Orbit

With SYMGENI we confirmed the orbital period determined from the radial velocities and then computed independent solutions of the two data sets. The separate radial-velocity and spectropolarimetric circular orbits have two elements in common, P and T_0 , which are reasonably consistent. However, the combined solution, instead of finding an intermediate period, produced a period that is shorter, although by only 1 or 2σ , than that determined for either separate solution. The two data sets were not obtained simultaneously, and Julian date plots of the two data sets, fitted with the two independently determined periods, show that both longer periods drift out of phase over the time span connecting the spectropolarimetric and velocity data. Thus, in the combined solution there is a greater increase in the residuals than one would expect from just reducing the number of free parameters.

Because of this result, we took a closer look at our data and its analysis. There are only six spectropolarimetric observations, and so we examined whether increasing the errors assigned to those data would significantly change the orbital solution. Even in a joint solution where the relative weights of the spectropolarimetric data were decreased by a factor of 5, the orbital elements were not significantly changed. Turning to the radial velocities, we note that V455 Sco has a spectral class of M6.5, and so, as discussed in Section 4, we estimate that up to half of the velocity residuals may result from pulsation. For the radial-velocity orbit the standard error of an observation of unit weight is 1 km s^{-1} , which is similar to or less than that of other symbiotic orbits that we have analyzed (e.g., Fekel et al. 2007). So, pulsational velocity variations are not a large contributor to the velocities. Thus, we can find no obvious problem in our data that would cause the increased errors in the combined solution (Table 3) of the two data sets. However, as mentioned above, the period differences of the various solutions are only at the $1-2\sigma$ level, and the extra parameter of particular astrophysical interest that results from the inclusion of the spectropolarimetric data, the orbital inclination, is quite insensitive to the weighting schemes or other details.

In Figure 4, we plot both the line polarization data and the radial velocities as a function of Julian date and compare the

Table 3
Orbital Elements and Related Parameters of V455 SCO

Parameter	Spectroscopic orbit	Combined orbit
P (days)	1443 ± 19	1397.8 ± 5.9
T_0 (HJD)	$2,452,987.2 \pm 9.1$	$2,452,991.0 \pm 9.4$
γ (km s^{-1})	-77.78 ± 0.24	-77.90 ± 0.23
K (km s^{-1})	8.00 ± 0.33	7.93 ± 0.32
e	0.0 adopted	0.0 adopted
Ω (deg)	...	169.49 ± 0.75
i (deg)	...	94.3 ± 1.4
$a \sin i$ (10^6 km)	159.4 ± 7.0	152.4 ± 6.2
$f(m)$ (M_\odot)	0.0777 ± 0.0097	0.0724 ± 0.0087
Velocity standard deviation (km s^{-1})	1.0	1.3

Note. An inclination greater than 90° indicates that the position angle decreases with time, corresponding to retrograde motion.

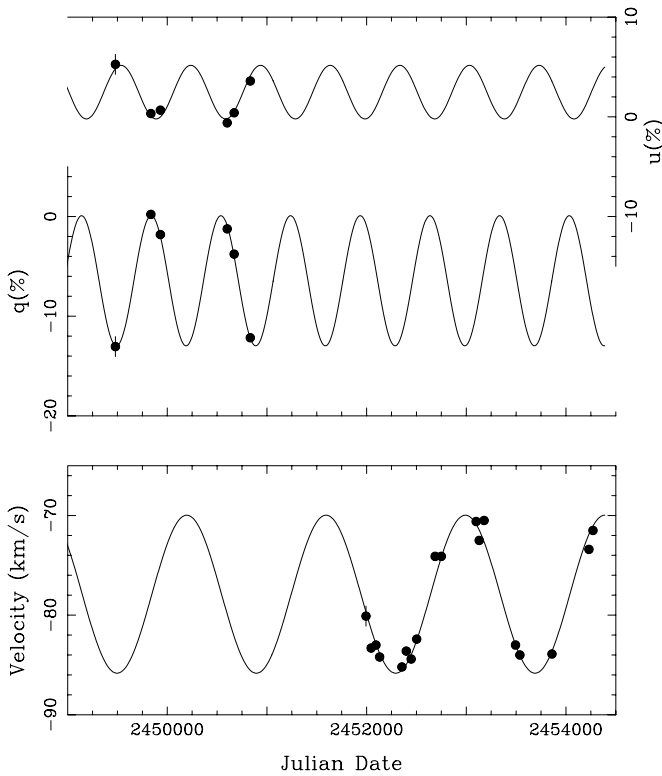


Figure 4. Upper panel: line polarization data (filled circles) of V455 Sco plotted as a function of Julian date. Lower panel: radial velocities (filled circles) of V455 Sco plotted as a function of Julian date. The solid lines in the two panels are from our best-fit combined solution. Representative error bars are shown on the first spectropolarimetric and velocity observations.

data with our combined solution fit. This shows the range of the two data sets, which do not overlap. Orbital phases for the velocity observations and velocity residuals to the final solution are given in Table 2. Table 4 lists similar quantities for the normalized Stokes parameters. In Figure 5 the velocities and computed velocity curve are compared in a phase plot of the orbit, where zero phase is a time of maximum velocity.

5.4. Emission-Line Orbit

Symbiotics in general display many strong emission lines from an ionized nebula (Mikołajewska 2003), and several nebular regions are usually postulated including one surrounding the hot component (e.g., Dobrzycka et al. 1993). Thus, it is possible

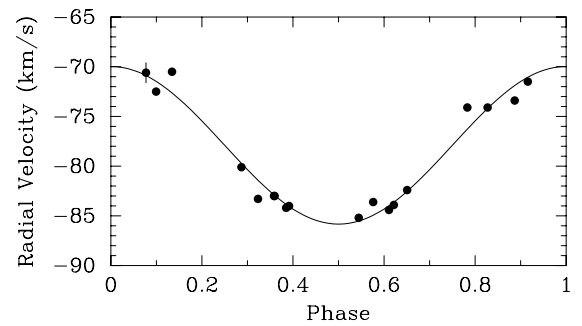


Figure 5. A phase plot of our V455 Sco radial velocities (filled circles) compared to the combined solution fit (solid line). Zero phase is a time of maximum velocity. The rms value, resulting from the velocity fit, is shown as an error bar on the first velocity.

Table 4
Normalized Stokes Parameters of V455 SCO

JD	q (%)	$(O - C)_q$ (%)	u (%)	$(O - C)_u$ (%)
2,400,000 +				
49,480	-13.05	-0.10	5.27	0.45
49,836	0.21	0.13	0.33	0.26
49,931	-1.81	0.19	0.67	0.68
50,601	-1.24	-0.32	-0.60	-0.42
50,671	-3.77	0.26	0.41	-0.13
50,833	-12.17	0.03	3.60	-0.51

that some emission lines may at least partially reflect the motion of the secondary.

After determining our combined orbit for the M giant we examined the velocities of the Paschen δ and He II emission lines in the $1 \mu\text{m}$ region (Table 5). The Paschen δ lines are relatively symmetric but some of the He II lines are not. When multiple blended components of an emission feature are evident, the listed velocity is that of the strongest component. Although the multiple emission components result in line asymmetries, we note that the emission features at phases closest to maximum and minimum velocity are reasonably symmetric.

Mikołajewska et al. (1989) stated that in symbiotics the He II emission lines should follow the hot component. In Figure 6, the computed M giant orbit is compared with the two sets of emission-line velocities. Our seven spectra cover nearly one orbital cycle, and except for the most recent observation, the velocities of the H I and He II emission features are similar at each phase. In addition, compared with the M giant orbit,

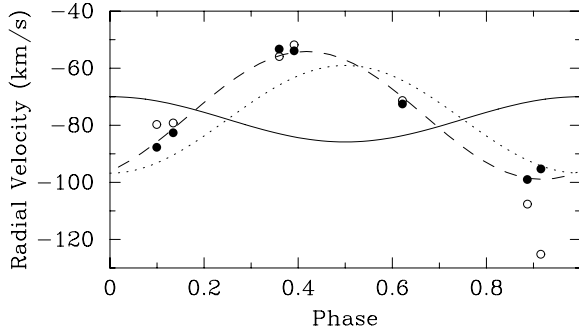


Figure 6. A phase plot of our V455 Sco emission radial velocities (filled circles: He II; open circles: H I) compared to the combined solution fit for the M giant (solid line) and the forced fit curve for the He II emission lines (dotted line), which requires their orbit to be 180° out of phase with the M giant orbit. The best fit to the He II emission-line velocities (dashed line) is also shown. Zero phase is a time of maximum velocity of the M giant.

Table 5
Emission-Line Radial Velocities of V455 SCO

HJD	Phase	H I velocity (km s^{-1})	He II velocity (km s^{-1})	He II $O - C$ (km s^{-1})	He II $(O - C)_{\text{ps}}$ (km s^{-1})
2,400,000 +					
53,129.883	0.099	-79.7	-87.7	5.5	-1.9
53,178.852	0.134	-79.2	-82.5	7.9	-1.3
53,493.913	0.360	-55.9	-53.3	12.6	2.3
53,537.815	0.391	-51.8	-53.9	9.4	0.5
53,859.925	0.622	-71.3	-72.5	-8.2	-2.4
54,230.787	0.887	-107.6	-99.0	-6.8	-0.5
54,270.822	0.916	-125.2	-95.3	-1.1	3.6

the emission velocities appear to be roughly 180° out of phase, indicating that they are indeed associated with the hot component. Thus, we obtained an orbital solution in which we adopted the elements of the M giant and solved for the semiamplitude of the He II emission line. The resulting mass ratio for the red giant and putative white dwarf, $M_{\text{rg}}/M_{\text{wd}}$, is 2.4 ± 0.5 , a value that is similar to that suggested for most symbiotics (Mikołajewska 2003), but the emission-line residuals for this solution (Table 5) are large, typically 5 to 12 km s^{-1} , and also deviate systematically because the emission-line velocities are not exactly 180° out of phase with the M giant solution. A circular orbit, determined for the He II emission lines alone with the period fixed at that of the M giant orbit, produced a very modest phase shift of 0.082 and greatly reduced the residuals (Table 5, $(O - C)_{\text{ps}}$). This second emission-line fit significantly decreased the rms from 8.1 to 2.1 km s^{-1} . Adopting this improved fit results in a larger mass ratio of 2.8 ± 0.4 . However, as we demonstrate in Section 5.5, neither of these two mass ratios is consistent with other properties of the stars.

5.5. Discussion

The orbital elements of the combined interferometric and red giant radial-velocity solution provide us with very useful information. From the spectroscopic elements we compute a value of $0.072 M_\odot$ (Table 3) for the mass function, $f(m)$. The mass function can also be written as

$$f(m) = (m_{\text{wd}}^3 \sin^3 i) / (m_{\text{rg}} + m_{\text{wd}})^2, \quad (1)$$

where m_{wd} is the mass of the putative white dwarf, m_{rg} is the mass of the red giant, and i is the orbital inclination. Because the inclination is known, an adopted white dwarf mass results

Table 6
Possible Masses of V455 SCO

M_{wd} (M_\odot)	M_{rg} (M_\odot)	$M_{\text{rg}}/M_{\text{wd}}$	Red giant age ^a (yr)
0.4	0.54	1.34	$> 15 \times 10^9$
0.5	0.81	1.62	$> 15 \times 10^9$
0.6	1.12	1.87	12×10^9
0.7	1.47	2.10	4×10^9
0.8	1.85	2.31	2×10^9
0.9	2.26	2.51	1×10^9
1.0	2.70	2.70	0.9×10^9
1.1	3.17	2.88	0.6×10^9
1.2	3.67	3.06	0.4×10^9

Note. ^a Age of the red giant at the start of the AGB (Vassiliadis & Wood 1993).

in a specific red giant mass. In Table 6, we list white dwarf masses ranging from 0.4 to $1.2 M_\odot$. For each white dwarf mass the corresponding M giant mass and mass ratio are given. As determined below, the luminosity of the red giant places it on the AGB. Thus, the age at the start of the AGB, taken from Vassiliadis & Wood (1993), is listed for the red giant in each combination.

The possible mass ranges of the two components are restricted. The most numerous white dwarfs are those that have atmospheric compositions primarily of hydrogen and are given the spectral classification of DA. The mass distribution of such white dwarfs has three components. The dominant peak, containing 75% of the stars, is at a mass of $0.6 M_\odot$, while a low-mass component is centered near $0.4 M_\odot$ and a broader high-mass component above about $0.8 M_\odot$ also exists (Liebert et al. 2005). Both the low-mass and high-mass white dwarfs have been created by special circumstances. The low-mass white dwarfs are made when helium core ignition fails to occur because of mass lost during the common envelope phase in a close binary. These stars are often double-degenerate systems (Marsh et al. 1995). The high-mass systems are thought to result from the merger of two white dwarfs in close binary evolution (e.g., Marsh et al. 1997). Thus, the circumstances that create low-mass and high-mass white dwarfs do not apply to most symbiotic stars.

Another important factor in determining the masses of the components is the age of V455 Sco. Symbiotics are members of the old disk population and so are low-mass stars (Wallerstein 1981). For V455 Sco, the large center of mass velocity of -77.9 km s^{-1} is certainly consistent with old disk membership.

Examining the mass combinations listed in Table 6, we conclude that the V455 Sco system cannot contain low-mass white dwarfs of 0.4 or $0.5 M_\odot$ not only because of the evolutionary scenario for their creation mentioned above, but also because the masses of the corresponding red giant components are so low that they would not evolve to the AGB stage during the age of the universe. For high-mass white dwarfs, masses $> 0.8 M_\odot$, the corresponding red giant components have masses $\geq 1.85 M_\odot$. Such massive giants have evolved from B or A main-sequence stars and are relatively young (Table 6). Thus, their ages are at odds with the system's old disk membership. We note that the mass ratio of 2.8, resulting from our best emission-line orbital solution, produces a high-mass white dwarf, $1.05 M_\odot$, and an M giant with a mass of $2.9 M_\odot$. So, the creation mechanism for high-mass white dwarfs, mentioned above, and the young ages of the red giant components preclude this result. Following the Goldilocks paradigm (e.g., Opie & Opie 1974), a white dwarf

mass of $0.6 M_{\odot}$, which is at the peak of the DA white dwarf mass distribution (Madej et al. 2004; Liebert et al. 2005), appears to be just right, producing an M giant mass of $1.12 M_{\odot}$, consistent with its status as an old disk system (Wallerstein 1981). Those masses result in a mass ratio of 1.9.

Based on the work of Zahn (1977), Schmutz et al. (1994) and Mürset et al. (2000) have argued that in most S-type symbiotics the giant star is synchronously rotating. If that is the case, then the projected rotational velocity of the late-type giant can be used to estimate its radius. To determine $v \sin i$ for the M giant, we measured the full-width at half-maximum of a few atomic features observed on the higher-resolution Phoenix 2.223 μm spectrum. We also measured the same lines in several late-type giants with known $v \sin i$ values. With the latter set of stars, we produced an empirical broadening calibration similar to that of Fekel (1997). Using the calibration and an adopted macroturbulence of 3 km s^{-1} , from two spectra we determined $v \sin i = 7.5 \pm 1 \text{ km s}^{-1}$ for the M giant component of V455 Sco. From our orbital solution the inclination is 94° . If we assume, as is generally done, that the orbital and rotational inclinations are equal, then the equatorial rotational velocity is also 7.5 km s^{-1} . The assumption of synchronous rotation results in an M giant radius of $207 \pm 28 R_{\odot}$.

This radius can be compared to the effective radius of the Roche lobe, which depends on the mass ratio and separation of the components. Adopting masses of 1.1 and $0.6 M_{\odot}$, Equation (2) of Eggleton (1983) produces an effective Roche-lobe radius of $271 R_{\odot}$ for the M giant. Thus, the giant fills a rather large fraction, $\sim 75\%$, of its Roche lobe. Given its relatively late spectral class of M6.5, perhaps this is not surprising, since the median radius of M giants increases with later spectral class (Dumm & Schild 1998). However, Mürset & Schmid (1999) found only one symbiotic binary out of a sample of 30 that was not well detached. The estimated radii of most of the 12 systems examined by Fekel et al. (2003) fill less than 50% of their Roche lobes and so are also well detached. An M giant would have its largest radius while on the AGB, but the lifetime of an M giant on the AGB is significantly shorter than its lifetime as a first-ascent giant branch star (Vassiliadis & Wood 1993). This fact, combined with the result that symbiotics are generally well-detached systems, argues that most symbiotics are first ascent red giants.

From our adopted spectral class of M6.5 (Mürset & Schmid 1999) we assume an effective temperature of 3300 K (Dyck et al. 1996). That, combined with our computed radius, results in a luminosity of $4550 L_{\odot}$, leading to $M_{\text{bol}} = -4.4 \text{ mag}$. Comparison with the theoretical predictions of Vassiliadis & Wood (1993) indicates that the M giant is an AGB star and may be undergoing thermal pulses. The mass loss rate of $1.7 \times 10^{-6} M_{\odot} \text{ yr}^{-1}$ (Seaquist et al. 1993) appears to be moderate. This fact plus the luminosity suggest a mass in excess of $1 M_{\odot}$ for the M giant, in accord with our preferred value of $1.1 M_{\odot}$.

To estimate the distance to V455 Sco, we adopted its K mag and $J - K$ color from Munari et al. (1992). We then used the analytic expression of Bessell & Wood (1984), involving that color, to obtain a bolometric correction at K . This, combined with our value of M_{bol} , produces $M_K = -7.66 \text{ mag}$ and results in a distance of 5.4 kpc if reddening is ignored. Including an extinction value of 0.5 mag decreases the distance to 4.3 kpc. The galactic latitude places the star 4° above the Galactic plane, while its longitude is within 9° of the Galactic center. Thus, the distance and position of V455 Sco toward the center of the

Milky Way is consistent with its membership in an older stellar population.

The inclination of $94^{\circ} \pm 1^{\circ}$ is well determined and indicates that the system is seen very nearly edge on, so despite the rather long orbital period of 3.8 yr, eclipses are expected. Eclipses occur if

$$a \cos i < R_{\text{rg}} + R_{\text{wd}}, \quad (2)$$

where a is the semimajor axis of the binary, i is the orbital inclination, and R is the radius of the red giant and white dwarf components. Using Kepler's third law and our adopted masses, we compute a semimajor axis of $627.6 R_{\odot}$. Compared to the radius of the M giant, that of the white dwarf is negligible, and so we find that the stars eclipse for inclinations between 71° and 119° . Major changes to the masses and even reducing the radius by a factor of 2 do not alter the conclusion that the system eclipses. From our combined solution the ephemeris for conjunctions with the M giant in front, which corresponds to times of mid-eclipse, is

$$T_{\text{conj}}(\text{HJD}) = 2,452,641.5(\pm 9) + 1398(\pm 6)E,$$

where E is an integer number of cycles.

The above ephemeris is for the eclipse of the putative white dwarf by the M giant. The very small size of the white dwarf and its luminosity at visual wavelengths means that the visual flux change caused by an eclipse of the white dwarf will be very small, less than 0.01 mag. However, an extended hot disk (e.g., Hutchings et al. 1983) would be easily observed at optical wavelengths. A search of the literature for evidence of the eclipses produces few modern observations. V455 Sco is not found in the All Sky Automated Survey (Pojmanski 2002) photometric database.⁶ Although a light curve for another southern symbiotic, BX Mon, was produced from observations collected by the Royal Astronomical Society of New Zealand, Variable Star Section (Dumm et al. 1998), no observations are available for V455 Sco (P. Loader 2007, private communication). Sokoloski (2003) urged optical monitoring of symbiotic stars to advance the study of accretion and jets. His Table 1 lists the symbiotics already in the AAVSO international database but unfortunately only a few measurements of V455 Sco have been obtained. By far the most numerous observations are those obtained from the Harvard College Observatory photographic plates (Figure 1, Swope 1940). Her data of V455 Sco (HV 7869) cover nearly 50 yr, but the light curve often is very fragmentary. Nevertheless, it shows that at times V455 Sco reached $m_{\text{pg}} \sim 13 \text{ mag}$ and had light variations of up to 4 mag, so the active hot component that is eclipsed presumably includes an accretion disk (Mikołajewska 2003). From about 1925 to 1937 the observations are the most numerous. During this period there are two significant extended brightness decreases of 2 mag or more that are roughly 1400 days apart, indicating that the system is eclipsing. However, one cycle later there is not another confirming brightness drop. Instead, the star appears to go into outburst mode, brightening by $\sim 2 \text{ mag}$. Adopting a mid-eclipse Julian date of 2,425,800 from Swope's plotted data, a period of 1412 days, which is about 2σ from our adopted period, is required to produce our mid-eclipse epoch of Julian date 2,452,641.5. Photometry of the eclipse could be a powerful tool in understanding the size and orientation of the disk.

⁶ <http://www.astrouw.edu.pl/~gp/asas/asas.html>.

6. SS 73-90 = M1-21 = HEN 2-247

6.1. Short History

Minkowski (1946) reported the results of additional observations of objects that showed H α emission but little or no continuum on Mount Wilson Observatory objective-prism survey plates. Minkowski (1946) included the object, later designated as M1-21, with about 70 others that he classified as planetary nebulae. Henize (1967) listed it in his catalog of southern planetary nebulae, providing a bit of information about the strength of its H α emission. Using moderately deep, low-dispersion objective-prism spectra, Sanduleak & Stephenson (1973) surveyed the southern Milky Way to search for luminous and emission-lined stars. They identified star number 90 in their 1973 list as a Z-Andromodae-like star, marking the first time that this object was classified as a symbiotic star. Because it does not have a variable star name, we have chosen to use the designation from the list of Sanduleak & Stephenson (1973), SS 73-90, as the name of the system. Following up on the work of Sanduleak & Stephenson (1973), Allen (1978) acquired a low-dispersion slit spectrum of SS 73-90. He also classified it as a symbiotic star, stating that it had strong TiO bands, the He II emission at 4686 Å was weaker than H β , and numerous weak forbidden lines were visible.

Allen (1980) called its spectral class M2 from a spectrum at 2 μ m. Later, Mürset & Schmid (1999) gave it an M6 classification, which we have adopted. Mikołajewska et al. (1997) estimated an upper limit of M1 for its spectral class. They also provided a limited analysis of SS 73-90, determining an approximate hot component temperature and luminosity and the system distance.

SS 73-90 was included in the symbiotic star catalog of Allen (1984), where a low-dispersion spectrum was shown, as well as the more recent catalog of Belczyński et al. (2000). In both catalogs it is listed as M1-21, although in Belczyński et al. (2000), its various other designations are also given.

In obtaining orbital solutions for SS 73-90 from their spectropolarimetric observations, Harries & Howarth (2000) found a bimodal period distribution with a period of about 900 days being marginally preferred statistically to a period of about 3000 days. They stated that additional observations were needed to confirm the 900 day orbit.

6.2. Spectroscopic Orbit

From 2001 May to 2007 June we obtained 17 radial velocities of SS 73-90 (Table 7), which cover nearly 2.5 orbital cycles. An analysis of these velocities produced an initial period of 911 days, which is similar to the value of 892 days that was favored by Harries & Howarth (2000). Adopting this period, we obtained preliminary orbital elements with BISP, which were refined with SB1. Because of the low orbital eccentricity of 0.15 ± 0.03 , we used SB1C to determine a circular-orbit solution. As suggested by the relatively small uncertainty of the eccentricity, the tests of Lucy & Sweeney (1971) indicated that the eccentric orbit is to be preferred, so it is given in Table 8.

6.3. Combined Orbit

With SYMGENI we confirmed the orbital period determined from the radial velocities and then computed independent solutions of the two data sets. Because the spectropolarimetric measurements have difficulty constraining some of the orbital

Table 7
Radial Velocities of SS 73-90

HJD 2,400,000 +	Phase	Velocity (km s ⁻¹)	O - C (km s ⁻¹)	Observatory
52,049.129	0.336	82.1	0.4	MSO
52,096.988	0.390	81.4	-0.5	MSO
52,353.273	0.675	91.0	0.5	MSO
52,400.146	0.727	93.1	0.1	MSO
52,448.963	0.782	95.9	0.2	MSO
52,507.029	0.846	99.0	0.6	MSO
52,687.876	0.048	93.8	-0.6	Gemini S
52,749.847	0.117	89.2	-0.2	Gemini S
52,866.516	0.247	82.9	0.0	Gemini S
53,098.836	0.505	83.9	-0.2	Gemini S
53,129.919	0.540	85.6	0.5	KPNO
53,179.799	0.595	87.5	0.4	KPNO
53,493.979	0.945	97.9	-1.5	KPNO
53,537.853	0.994	99.4	1.7	KPNO
53,899.891	0.397	81.3	-0.6	KPNO
54,230.930	0.766	95.0	0.1	KPNO
54,271.883	0.812	96.1	-0.9	KPNO

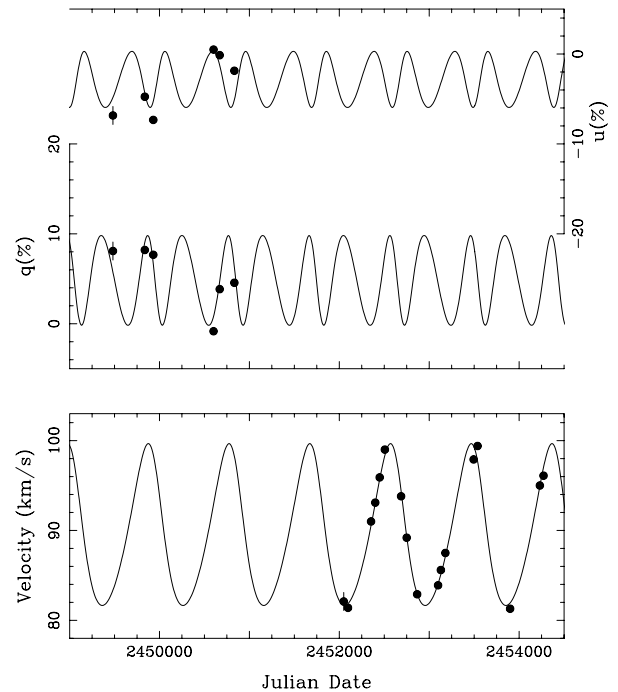


Figure 7. Upper panel: line polarization data (filled circles) of SS 73-90 plotted as a function of Julian date. Lower panel: radial velocities (filled circles) of SS 73-90 plotted as a function of Julian date. The solid lines in the two panels are from our best-fit combined solution. Representative error bars are shown on the first spectropolarimetric and velocity observations.

parameters, the primary issue in combining those observations with the radial velocities is the relative weighting of the two data sets. With standard deviations of 2.6% for the spectropolarimetric measurements and 0.8 km s^{-1} for the velocities, we adopt the final joint orbital solution, which is presented in Table 8. For SS 73-90, the period of the joint solution is intermediate between the independent spectropolarimetric and radial-velocity solutions.

In Figure 7, we plot both the line polarization data and the radial velocities as a function of Julian date and compare the data with our combined solution fit. This shows the range of the two data sets, which do not overlap. Orbital phases for the velocity observations and velocity residuals to the final solution are given

Table 8
Orbital Elements and Related Parameters of SS 73-90

Parameter	Spectroscopic orbit	Combined orbit
P (days)	907.6 ± 6.5	898.0 ± 4.7
T (HJD)	$2,452,661.6 \pm 29.2$	$2,452,645.1 \pm 33.2$
γ (km s^{-1})	89.56 ± 0.19	89.54 ± 0.27
K (km s^{-1})	8.97 ± 0.29	9.00 ± 0.38
e	0.153 ± 0.031	0.165 ± 0.040
ω (deg)	50.3 ± 12.2	41.5 ± 14.0
Ω (deg)	...	74.8 ± 4.4
i (deg)	...	96.7 ± 7.1
$a \sin i$ (10^6 km)	110.6 ± 3.7	109.6 ± 4.7
$f(m)$ (M_{\odot})	0.0657 ± 0.0064	0.0652 ± 0.0084
Velocity standard deviation (km s^{-1})	0.8	1.0

Note. An inclination greater than 90° indicates that the position angle decreases with time, corresponding to retrograde motion.

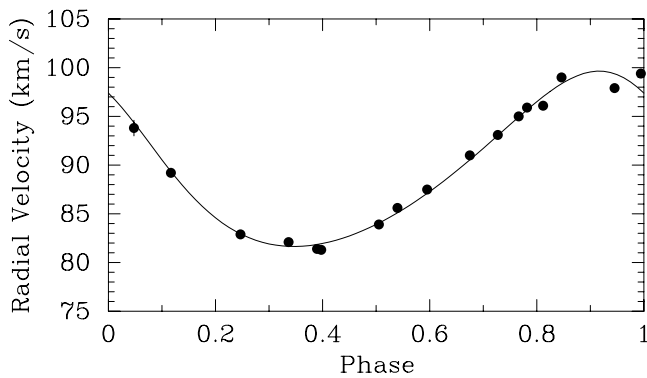


Figure 8. A phase plot of our SS 73-90 radial velocities (filled circles) compared to the combined solution fit (solid line). Zero phase is a time of periastron passage. The rms value, resulting from the velocity fit, is shown as an error bar on the first velocity.

Table 9
Normalized Stokes Parameters of SS 73-90

JD 2,400,000 +	q (%)	$(O - C)_q$ (%)	u (%)	$(O - C)_u$ (%)
49,482	8.09	2.34	-6.83	-1.99
49,837	8.20	-0.85	-4.75	-0.42
49,931	7.67	0.99	-7.33	-2.07
50,601	-0.84	-1.63	0.50	0.23
50,670	3.84	-0.93	-0.13	1.14
50,833	4.56	-1.75	-1.86	3.23

in Table 7. Table 9 lists similar quantities for the normalized Stokes parameters. In Figure 8, the velocities and computed velocity curve from our combined orbit fit are compared. Zero phase is a time of periastron.

6.4. Emission-Line Orbit

After determining our combined orbit for the M giant of SS 73-90 we examined the velocities of the Paschen δ and He II emission lines in the $1 \mu\text{m}$ region. While measurement of the He II feature was straightforward, because its emission profile generally consisted of a dominant component plus very weak red or blue wings, analysis of the H I line was more problematic because it usually had blended components of similar intensity. Thus, the H I line in six of the seven spectra was fitted with a double Gaussian. Table 10 lists the emission-line velocities, giving two velocities for the H I line when appropriate. In

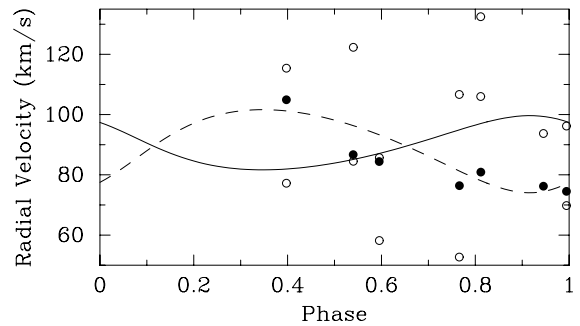


Figure 9. A phase plot of our SS 73-90 emission radial velocities (filled circles: He II; open circles: H I) compared to the combined solution fit for the M giant (solid line) and the forced fit curve for the He II emission lines (dashed line). Zero phase is a time of periastron passage.

Table 10
Emission-Line Radial Velocities of SS 73-90

HJD 2,400,000 +	Phase	H I velocity (km s^{-1})	He II velocity (km s^{-1})	He II $O - C$ (km s^{-1})
53129.919	0.540	84.5	86.7	-9.6
	0.540	122.3
53179.799	0.595	58.2	84.4	-8.9
	0.595	85.7
53493.979	0.945	93.7	76.2	1.8
	53537.853	0.994	69.8	74.5
53899.891		0.994	96.2	...
	0.397	77.2	104.9	3.7
54230.930	0.397	115.4
	0.766	52.7	76.4	-4.9
54271.883	0.766	106.7
	0.812	106.0	80.9	2.8
	0.812	132.5

Figure 9, the computed M giant orbit is compared with the velocities of the H I and He II emission features. The H I emission velocities appear to scatter wildly about the phase plot. On the other hand the He II velocities roughly mirror the M giant orbit, and so appear to be associated with the hot component. Although our seven spectra are not as well distributed in orbital phase as those for V455 Sco, we nevertheless computed a joint absorption and emission-line orbital solution. As we did for V455 Sco, we adopted the elements of the M giant and solved for only the semi-amplitude of the He II emission-line velocities. That solution produced a mass ratio, $M_{\text{rg}}/M_{\text{wd}}$, of 1.5 ± 0.3 .

Table 11
Possible Masses of SS 73-90

M_{wd} (M_{\odot})	M_{rg} (M_{\odot})	$M_{\text{rg}}/M_{\text{wd}}$	Red giant age ^a (yr)
0.4	0.58	1.45	$> 15 \times 10^9$
0.5	0.87	1.74	$> 15 \times 10^9$
0.6	1.20	2.00	8×10^9
0.7	1.57	2.24	3×10^9
0.8	1.97	2.46	2×10^9
0.9	2.41	2.68	1×10^9
1.0	2.87	2.87	0.8×10^9
1.1	3.37	3.06	0.5×10^9
1.2	3.89	3.24	0.4×10^9

Note. ^a Age of the red giant at the start of the AGB (Vassiliadis & Wood 1993).

6.5. Discussion

The information that is available for SS 73-90 is similar to that for V455 Sco. From Table 8 the mass function of the M giant orbit is $0.065 M_{\odot}$, and the orbital inclination is 97° . Because the inclination is known, the mass function equation produces a specific red giant mass for each adopted white dwarf mass. In Table 11, we list white dwarf masses ranging from 0.4 to $1.2 M_{\odot}$. For each white dwarf mass the corresponding red giant mass and mass ratio are given. Although SS 73-90 is not as luminous as V455 Sco, we conclude below that it is likely an AGB star. Therefore, the age at the start of the AGB, taken from Vassiliadis & Wood (1993), is listed for the red giant in each combination.

SS 73-90 has a large systemic velocity of 89.5 km s^{-1} , indicating that it is a member of the old disk population. Thus, the red giant is a low-mass star (Wallerstein 1981).

Examining the various mass combinations in Table 11, the same arguments that we used for V455 Sco, the creation mechanisms for white dwarfs of various masses, the age of the red giant component, and the old disk membership of the system, cause us to reject the low-mass and high-mass white dwarf possibilities for SS 73-90. For the particular case of our joint absorption and emission-lined orbital solution, the mass ratio of 1.53 results in masses of 0.43 and $0.66 M_{\odot}$ for the white dwarf and red giant, respectively. We conclude that the SS 73-90 system cannot contain such a combination not only because of the low-mass white dwarf creation scenario mentioned in Section 5.5, but also because the mass of the corresponding red giant component is so low that it would not evolve to the AGB stage during the age of the universe. As a result, for the components we adopt the typical white dwarf mass of 0.6 and the corresponding $1.2 M_{\odot}$ for the M giant, which results in a mass ratio of 2.0.

As noted in Section 5.5, Schmutz et al. (1994) and Mürset et al. (2000) have argued that in most S-type symbiotics the giant star is synchronously rotating. However, the orbit of SS 73-90 is not circular but has a modest eccentricity of 0.16. Thus, the rotational angular velocity of the M giant will synchronize with that of the orbital motion at periastron, a condition called “pseudosynchronous rotation” (Hut 1981). With Equation (42) of Hut (1981) we calculated a pseudosynchronous period of 771 days.

With the same procedure that we used for V455 Sco, from two spectra we determined $v \sin i = 9 \pm 1 \text{ km s}^{-1}$ for the M giant component of SS 73-90. The orbital inclination is so high that, with the assumption that the orbital and

rotational inclinations are equal, we simply adopt the value of 9 km s^{-1} for the equatorial rotational velocity. Combining the pseudosynchronous period with the rotational velocity results in a radius of $137 \pm 15 R_{\odot}$.

The Roche-lobe radius of the giant depends on the separation of the stars and their mass ratio. However, the orbit of SS 73-90 is not circular, so the separation will vary. Nevertheless, the eccentricity is not extremely large, and we can get an estimate of the Roche lobe by adopting the smaller periastron separation rather than the semimajor axis. This produces a minimum Roche-lobe radius of $175 R_{\odot}$. Thus, at periastron, the M6 giant of SS 73-90 appears to fill about 75% of its Roche lobe, similar to the result for V455 Sco. Of course, as the separation of the stars increases the size of the M giant’s Roche lobe will also increase, decreasing the percentage that is filled.

From our adopted spectral class of M6 (Mürset & Schmid 1999) we assume an effective temperature of 3380 K (Dyck et al. 1996) for SS 73-90. That, combined with our computed radius, results in a luminosity of $2200 L_{\odot}$, leading to $M_{\text{bol}} = -3.6 \text{ mag}$, nearly a magnitude fainter than V455 Sco. Comparison with the theoretical predictions of Vassiliadis & Wood (1993) indicates that the M giant is likely an AGB star. According to Seaquist et al. (1993), the mass loss rate is $1.7 \times 10^{-7} M_{\odot} \text{ yr}^{-1}$, which is an order of magnitude less than that of V455 Sco. This fact plus the luminosity and its old disk population membership suggest a mass of $1-2 M_{\odot}$ for the M giant, in accord with our preferred value of $1.2 M_{\odot}$.

To estimate the distance to SS 73-90, we adopted its K mag and $J - K$ color from Munari et al. (1992). We then used the analytic expression of Bessell & Wood (1984), involving that color, to obtain a bolometric correction at K . This, combined with our value of M_{bol} , produces $M_K = -6.81 \text{ mag}$ and results in a distance of 5.9 kpc if reddening is ignored. Including an extinction value of 0.5 mag decreases the distance to 4.7 kpc. The galactic latitude places the star 7° above the Galactic plane, while its longitude is within 7° of the Galactic center. Thus, the distance and position of SS 73-90 toward the center of the Galaxy is consistent with its membership in an older stellar population.

The orbit of SS 73-90, like that of V455 Sco, has a high inclination, so the orbit is nearly edge on. Although the derived inclination of $97^{\circ} \pm 7^{\circ}$ is more uncertain than that of V455 Sco, the period of SS 73-90 is significantly shorter, just two-thirds that of V455 Sco. Following the same steps as we did for V455 Sco, and using our adopted parameters, but substituting the apastron separation for the semimajor axis, we find that eclipses of the white dwarf occur if the inclination is between 76° and 114° . Thus, it appears that SS 73-90 also eclipses.

From the elements of our joint solution the ephemeris for conjunctions with the M giant in front, which corresponds to times of mid-eclipse, is

$$T_{\text{conj}}(\text{HJD}) = 2,452,355(\pm 33) + 898(\pm 5)E,$$

where E represents an integer number of cycles. Once again, photometry of the eclipse could be a powerful tool in elucidating the size and orientation of the white dwarf accretion disk. However, SS 73-90 is generally rather faint. The All Sky Automated Survey photometric database (Pojmanski 2002) contains 272 observations of the region around SS 73-90 that were acquired from 2001 February through 2004 October. For the vast majority of those observations, the star was fainter than the limiting magnitude, $V = 15 \text{ mag}$, of the survey. Only on several occasions did it brighten to $V \leq 14 \text{ mag}$.

No observations are available from the RASNZ (P. Loader 2007, private communication) or are in the AAVSO database (Sokoloski 2003). In the latest of a series of papers Henden & Munari (2006) have provided photometric sequences and the astrometric position of SS 73-90 to facilitate CCD monitoring of it.

7. GENERAL DISCUSSION

7.1. Period–Eccentricity Distribution

The distribution of binaries in the period–eccentricity plane provides information about binary star evolution (Jorissen et al. 1998). Fekel et al. (2007) examined that distribution for 30 symbiotic binaries with spectroscopic orbits. They found that 81% of the binaries with periods less than or equal to 800 days have circular orbits. For periods greater than 800 days, only two of the nine systems have orbits that are circular. Both V455 Sco and SS 73-90 are in the longer-period group. Because V455 Sco has a circular orbit, the percentage of systems with circular orbits in that group is increased to 27%.

7.2. Eclipse Probabilities

The discovery that in both V455 Sco and SS 73-90 the late-M giant component should eclipse the presumed white dwarf suggests that eclipses are fairly common among symbiotic systems. The probability of eclipse for symbiotics can be readily computed. Mikołajewska (2007) presented a histogram of 63 symbiotic periods found either spectroscopically or photometrically, and a 1.9 year period appears representative for the S-type symbiotics. Mikołajewska (2007) also provides mass distributions for the hot components and late-type giants of symbiotic systems. A value of $2.1 M_{\odot}$ for the combined binary mass is typical, producing a semimajor axis of 2.0 AU from Kepler's third law. Equation (2) for the limiting inclination of an eclipse relates the inclination, semimajor axis, and stellar radii. Ignoring the very small radius of the presumed white dwarf, typical values for giant radii (Dumm & Schild 1998) are $50 R_{\odot}$ for an M0 III and $150 R_{\odot}$ for an M6 III. Integrating over a random distribution of inclination angles shows that the probability of an inclination greater than the limiting angle is $\cos(i_{\text{lim}})$. Thus for symbiotics with M0 giants, the probability of eclipse is about 1 in 9 and increases to about 1 in 3 for M6 giants.

Of the 32 systems with spectroscopic orbits, 27 listed in Mikołajewska (2003) and five more in Hinkle et al. (2006), Fekel et al. (2007), and this paper, there are 14 systems with components that are claimed to eclipse. This number is greater than expected given that at least half of M giants in the sample have spectral classes earlier than M5. However, among systems selected from a radial-velocity sample there is a bias toward detecting higher velocity amplitude systems, i.e., systems with larger inclinations. In addition, an accretion disk around the white dwarf would increase the size of the hot object that is eclipsed. These factors increase the probability of selecting eclipsing systems, since i_{lim} is typically in the range 70° – 80° . Thus, it is not surprising that we predict that both V455 Sco and SS 73-90 are eclipsing systems. Given the large fraction of eclipsing systems among the symbiotics, considerable information about symbiotic orbital periods can be expected from large area photometric sky survey databases (e.g., Gromadzki et al. 2007).

We thank the referee for suggestions that resulted in an improved paper. This paper is based in part on observations ob-

tained at the Gemini Observatory, which is operated by the Association of Universities for Research in Astronomy, Inc., under a cooperative agreement with the NSF on behalf of the Gemini partnership: the National Science Foundation (United States), the Particle Physics and Astronomy Research Council (United Kingdom), the National Research Council (Canada), CONICYT (Chile), the Australian Research Council (Australia), CNPq (Brazil), and CONICRT (Argentina). The observations were obtained with the Phoenix infrared spectrograph, which was developed and is operated by the National Optical Astronomy Observatory. The Gemini/Phoenix spectra were obtained as part of programs GS-2003A-DD-1, GS-2003B-DD-1, and GS-2004A-DD-1. This research has been supported in part by NASA grants NCC5-511 and NSF grant HRD-9706268 to Tennessee State University. We have made use of the SIMBAD database, operated by CDS in Strasbourg, France, as well as NASA's Astrophysics Data System Abstract Service.

REFERENCES

- Allen, D. A. 1978, *MNRAS*, **184**, 601
 Allen, D. A. 1980, *MNRAS*, **192**, 521
 Allen, D. A. 1984, *Proc. Astron. Soc. Aust.*, **5**, 369
 Barker, E. S., Evans, D. S., & Laing, J. D. 1967, *R. Obs. Bull.*, No. 130
 Batten, A. H., Fletcher, J. M., & MacCarthy, D. G. 1989, *Publ. Dom. Astrophys. Obs. Victoria*, **17**, 1
 Belczyński, K., Mikołajewska, J., Munari, U., Ivison, R. J., & Friedjung, M. 2000, *A&AS*, **146**, 407
 Berman, L. 1932, *PASP*, **44**, 318
 Bessell, M. S., & Wood, P. R. 1984, *PASP*, **96**, 247
 Bidelman, W. P. 1954, *ApJS*, **1**, 175
 Charbonneau, P. 1995, *ApJS*, **101**, 309
 Dobrzycka, D., Kenyon, S. J., & Mikołajewska, J. 1993, *AJ*, **106**, 284
 Dumm, T., Mürset, U., Nussbaumer, H., Schild, H., Schmid, H. M., Schmutz, W., & Shore, S. N. 1998, *A&A*, **336**, 637
 Dumm, T., & Schild, H. 1998, *New Astron.*, **3**, 137
 Dyck, H. M., Benson, J. A., van Belle, G. T., & Ridgway, S. T. 1996, *AJ*, **111**, 1705
 Eggleton, P. P. 1983, *ApJ*, **269**, 368
 Fekel, F. C. 1997, *PASP*, **109**, 514
 Fekel, F. C., Hinkle, K. H., & Joyce, R. R. 2003, in *ASP Conf. Ser.* 303, *Symbiotic Stars Probing Stellar Evolution*, ed. R. L. M. Corradi, J. Mikołajewska, & T. J. Mahoney (San Francisco, CA: ASP), **113**
 Fekel, F. C., Hinkle, K. H., Joyce, R. R., & Skrutskie, M. F. 2000a, *AJ*, **120**, 3255
 Fekel, F. C., Hinkle, K. H., Joyce, R. R., & Skrutskie, M. F. 2001, *AJ*, **121**, 2219
 Fekel, F. C., Hinkle, K. H., Joyce, R. R., Wood, P. R., & Lebzelter, T. 2007, *AJ*, **133**, 17
 Fekel, F. C., Joyce, R. R., Hinkle, K. H., & Skrutskie, M. F. 2000b, *AJ*, **119**, 1375
 Fitzpatrick, M. J. 1993, in *ASP Conf. Ser.* 52, *Astronomical Data Analysis Software and Systems II*, ed. R. J. Hanish, R. V. J. Brissenden, & J. Barnes (San Francisco, CA: ASP), **472**
 Garcia, M. R. 1986, *AJ*, **91**, 1400
 Glass, I. S., & van Leeuwen, F. 2007, *MNRAS*, **378**, 1543
 Gromadzki, M., Mikołajewska, J., Borawska, M., & Lednicka, A. 2007, *Balt. Astron.*, **16**, 37
 Harries, T. J., & Howarth, I. D. 1996, *A&AS*, **119**, 61
 Harries, T. J., & Howarth, I. D. 2000, *A&A*, **361**, 139
 Henden, A., & Munari, U. 2006, *A&A*, **458**, 339
 Henize, K. G. 1967, *ApJS*, **14**, 125
 Henize, K. G. 1976, *ApJS*, **30**, 491
 Hinkle, K. H., Fekel, F. C., Joyce, R. R., Wood, P. R., Smith, V., & Lebzelter, T. 2006, *AJ*, **641**, 479
 Hinkle, K. H., et al. 1998, *Proc. SPIE*, **3354**, 810
 Hogg, F. S. 1934, *Publ. AAS*, **8**, 14
 Hut, P. 1981, *A&A*, **99**, 126
 Hutchings, J. B., Cowley, A. P., Ake, T. B., & Imhoff, C. L. 1983, *ApJ*, **275**, 271
 Jorissen, A., Van Eck, S., Mayor, M., & Udry, S. 1998, *A&A*, **332**, 877
 Joyce, R. R. 1992, in *ASP Conf. Ser.* 23, *Astronomical CCD Observing and Reduction Techniques*, ed. S. Howell (San Francisco, CA: ASP), **258**
 Joyce, R. R., Hinkle, K. H., Meyer, M. R., & Skrutskie, M. F. 1998, *Proc. SPIE*, **3354**, 741
 Keenan, P. C., & McNeil, R. C. 1989, *ApJS*, **71**, 245
 Kenyon, S. J., & Webbink, R. F. 1984, *ApJ*, **279**, 252

- Lebzelter, T., & Hinkle, K. H. 2002, *A&A*, **393**, 563
- Liebert, J., Bergeron, P., & Holberg, J. B. 2005, *ApJS*, **156**, 47
- Lucy, L. B., & Sweeney, M. A. 1971, *AJ*, **76**, 544
- Madej, J., Nalezty, M., & Althaus, L. G. 2004, *A&A*, **419**, L5
- Marsh, M. C., Barstow, M. A., Buckley, D. A., Burleigh, M. R., Holberg, J. B., & Koester, D. 1997, *MNRAS*, **286**, 369
- Marsh, T. R., Dhillon, V. S., & Duck, S. R. 1995, *MNRAS*, **275**, 828
- Medina Tanco, G. A., & Steiner, J. E. 1995, *AJ*, **109**, 1770
- Merrill, P. W., & Burwell, C. G. 1950, *ApJ*, **112**, 72
- Mikołajewska, J. 2003, *Symbiotic Stars Probing Stellar Evolution*, ed. R. L. M. Corradi, J. Mikołajewska, & T. J. Mahoney (San Francisco, CA: ASP), 9
- Mikołajewska, J. 2007, *Balt. Astron.*, **16**, 1
- Mikołajewska, J., Acker, A., & Stenholm, B. 1997, *A&A*, **327**, 191
- Mikołajewska, J., Kenyon, S. J., & Mikołajewski, M. 1989, *AJ*, **98**, 1427
- Minkowski, R. 1946, *PASP*, **58**, 305
- Munari, U., Yudin, B. F., Taranova, O. G., Massone, G., Marang, F., Roberts, G., Winkler, H., & Whitelock, P. A. 1992, *A&AS*, **93**, 383
- Mürset, U., Dumm, T., Isenegger, S., Nussbaumer, H., Schild, H., Schmid, H. M., & Schmutz, W. 2000, *A&A*, **353**, 952
- Mürset, U., Nussbaumer, H., Schmid, H. M., & Vogel, M. 1991, *A&A*, **248**, 458
- Mürset, U., & Schmid, H. M. 1999, *A&AS*, **137**, 473
- Opie, I., & Opie, P. 1974, *The Classic Fairy Tales*, (New York: Oxford University Press)
- Percy, J. R., Wilson, J. B., & Henry, G. W. 2001, *PASP*, **113**, 983
- Pojmanski, G. 2002, *Acta Astron.*, **52**, 397
- Sanduleak, N., & Stephenson, C. B. 1973, *ApJ*, **185**, 899
- Scarfe, C. D., Batten, A. H., & Fletcher, J. M. 1990, *Publ. Dom. Astrophys. Obs. Victoria*, **18**, 21
- Schmid, H. M., & Schild, H. 2002, *A&A*, **395**, 117
- Schmutz, W., Schild, H., Mürset, U., & Schmid, H. M. 1994, *A&A*, **288**, 819
- Sequist, E. R., Krogulec, M., & Taylor, A. R. 1993, *ApJ*, **410**, 260
- Sokoloski, J. J. 2003, *J. Am. Assoc. Variable Star Obs.*, **31**, 89
- Swope, H. 1940, *Ann. Harvard Coll. Obs.*, **90**, 231
- Vassiliadis, E., & Wood, P. R. 1993, *ApJ*, **413**, 641
- Wackerling, L. R. 1970, *Mem. RAS*, **73**, 153
- Wallerstein, G. 1981, *The Observatory*, **101**, 172
- Webster, B. L., & Allen, D. A. 1975, *MNRAS*, **171**, 171
- Wolfe, R. H., Horak, H. G., & Storer, N. W. 1967, in *Modern Astrophysics*, ed. M. Hack (New York: Gordon & Breach), 251
- Wray, J. D. 1966, PhD Thesis, Northwestern Univ.
- Zahn, J.-P. 1977, *A&A*, **57**, 383